Next-Cycle Optimal Fuel Control for Cycle-to-Cycle Variability Reduction in EGR-Diluted Combustion

Bryan P. Maldonado, *Member, IEEE*, Brian C. Kaul, Catherine D. Schuman, *Senior Member, IEEE*, Steven R. Young, *Member, IEEE*, and J. Parker Mitchell, *Member, IEEE*

***Abstract*—Dilute combustion using exhaust gas recirculation (EGR) is a cost-effective method for increasing engine efficiency. At high EGR levels, however, its efficiency benefits diminish as cycle-to-cycle variability (CCV) intensifies. In this simulation study, cycle-to-cycle fuel control was used to reduce CCV by injecting additional fuel in operating conditions with sporadic misfires and partial burns. An optimal control policy was proposed that utilizes 1) a physics-based model that tracks in-cylinder gas composition and 2) a one-step-ahead prediction of the combustion efficiency based on a kernel density estimator. The optimal solution, however, presents a tradeoff between the reduction in combustion CCV and the increase in fuel injection quantity required to stabilize the charge. Such a tradeoff can be adjusted by a single parameter embedded in the cost function. Simulation results indicated that combustion CCV can be reduced by as much as 65% by using at most 1% additional fuel. Although the control design presented here does not include fuel trim to maintain $\lambda = 1$ for three-way catalyst compatibility, it is envisioned that this approach would be implemented alongside such an external controller, and the theoretical contribution presented here provides a first insight into the feasibility of CCV control using fuel injection.**

***Index Terms*—Automotive control, energy systems, grey-box modeling, stochastic optimal control.**

Manuscript received September 14, 2020; revised November 30, 2020; accepted December 6, 2020. Date of publication December 22, 2020; date of current version April 28, 2021. This work was supported in part by the UT-Battelle LLC with the U.S. DOE under Contract DE-AC05-00OR22725; in part by the DOE Office of Energy Efficiency and Renewable Energy (EERE), Vehicle Technologies Office; and in part by the Laboratory Directed Research and Development Program of ORNL. Recommended by Senior Editor R. S. Smith. *(Corresponding author: Bryan P. Maldonado.)*

Bryan P. Maldonado and Brian C. Kaul are with the Buildings and Transportation Science Division, Oak Ridge National Laboratory, Oak Ridge, TN 37830 USA (e-mail: maldonadopbp@ornl.gov; kaulbc@ornl.gov).

Catherine D. Schuman, Steven R. Young, and J. Parker Mitchell are with the Computer Science and Mathematics Division, Oak Ridge National Laboratory, Oak Ridge, TN 37830 USA (e-mail: schumancd@ornl.gov; youngsr@ornl.gov; mitchelljp1@ornl.gov).

Digital Object Identifier 10.1109/LCSYS.2020.3046433

I. Introduction

REGULATIONS on greenhouse gas emissions require engine efficiency improvements, especially in the short- to medium-term [1]. Exhaust gas recirculation (EGR) in stoichiometric spark-ignition engines is a cost-effective technology to increase efficiency by mainly reducing pumping work and heat transfer losses [2]. For a given condition the maximum amount of EGR is limited by improper levels of cycle-to-cycle variability (CCV). High levels of EGR affect the flame kernel development causing partial burns and misfires, exacerbating CCV. If such events were preventable, the EGR dilution limit could be extended, further increasing efficiency benefits [3]. At high dilution, CCV presents prior-cycle determinism thanks to the residual gas [4], [5]. Hence, predictive control could prevent misfires and partial burns to extend the benefits of high EGR dilution. Two actuators can be used to accomplish this task: spark advance and fuel injection. Modeling the influence of spark in combustion often requires empirical maps and lookup tables [6]. Previous studies have used spark control to operate at the dilution limit. However, misfires were assumed to be random and the deterministic effect of residual gas was not considered [7], [8]. On the other hand, fuel properties can be tied to the energy released during combustion, making it possible to use a physics-based model based on residual gas effects [9].

Symbol sequence statistics of the gross heat release Q_{gross}, introduced in [3], [5], [9], has been a powerful tool to quantify the controllability of partial burns and misfires. This technique utilizes discretized symbols (i.e., data binning) of Q_{gross} to reduce the random noise in the observations and identify deterministic patterns. The evidence of prior-cycle correlation indicates that a combustion event can influence the behavior of the next cycle. Therefore, a stochastic controller could use the symbol sequence histogram as the information state for a partially-observed Markov decision process. In this letter, we will consider a more general problem setup where the state, control, and observation spaces are continuous. The control policy, however, will be limited to a state feedback law by assuming full observation of the system. An optimal control problem will be formulated that attempts to reduce CCV by using small perturbations from the stoichiometric fuel value. The solution to the next-cycle control problem is presented

TABLE I
ENGINE CHARACTERISTICS AND OPERATING CONDITIONS

Bore × Stroke	86 [mm] × 86 [mm]
Compression ratio	9.2:1
Intake valve closing (IVC)	-110 [CAD]
Exhaust valve opening (EVO)	160 [CAD]
Engine speed	2000 [RPM]
Intake airflow	309 [g/min]
Injection timing	-300 [CAD]
Coolant/Intake temperatures	90/40 [°C]

using a model-based approach and statistical properties of the combustion efficiency. Simulated results show a promising reduction of CCV with minimum fuel consumption penalty.

The letter is organized as follows: Section II presents the engine experimental conditions. Section III details the non-parametric control-oriented model. Section IV defines the optimal control problem and presents the method to solve it. Finally, Section V shows the closed-loop simulations.

II. EXPERIMENTAL SETUP

Data were collected from a single-cylinder version of a 2[L] GM Ecotec LNF spark-ignition direct-injection engine fitted with an external EGR system. The experimental conditions are described in Table I. The engine speed and the fuel flow were kept constant for all conditions. Fresh airflow was adjusted according to a wide-band exhaust oxygen sensor to maintain a stoichiometric charge. The EGR fraction was increased from 10% to 16% to capture the transition from a stable to an unstable combustion behavior. The spark advance was varied in a wide range to capture the characteristics of the misfire limit and partial burn limit. The engine load, measured by the indicated mean effective pressure (IMEP), ranged between 5-6 [bar] and represents a typical mid-load cruising operation where EGR contributes to an increase in engine efficiency [2]. The EGR fraction was calculated using an intake oxygen sensor. The in-cylinder pressure was measured using a flush-mounted piezoelectric pressure transducer. Research-grade E10 gasoline known as RD5-87, representative of regular-grade market gasoline, was used. For each spark/EGR combination, a total of 5,000 engine cycles were recorded.

Typically, combustion CCV is quantified by the coefficient of variation (CoV) of IMEP. Figure 1 shows the CoV values of IMEP and Q_{gross} for all the spark/EGR combinations. The dashed line corresponds to the optimal combustion phasing of CA50 = 8 [CAD]. Here, CA50 denotes the crank angle location for 50% mass fuel burned. To maintain the optimal phasing, spark advance is needed to compensate for slower burning rates under high EGR. Note that the CoV values for IMEP and Q_{gross} follow a similar trend at conditions close to the optimal CA50. At retarded spark, however, the CoV values between these two variables show large discrepancies. This occurs because Q_{gross} is not as sensitive to phasing as IMEP and shows small variations with respect to spark.

Industry standards generally limit CCV to a maximum of 3% CoV of IMEP. Higher CoV values are caused by sporadic misfires ($Q_{\text{gross}} \leq 0$) and partial burns. In this letter, partial burns are defined as combustion events with lower than 75% of nominal Q_{gross}. Figure 1 shows the regions with misfires, partial burns, and complete combustion. Fuel consumption and

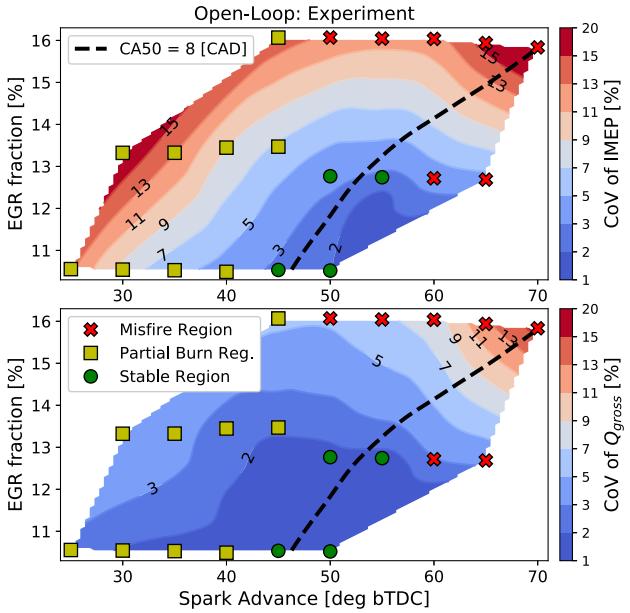

Fig. 1. Coefficient of variation for IMEP (top) and gross heat release Q_{gross} (bottom) during a spark/EGR sweep at constant engine speed.

emissions are minimized at the optimal CA50. Increasing EGR levels contribute to a further reduction in fuel consumption, until the stability limit is reached. This motivates the study of predictive control to avoid partial burns and misfires, extending the stable region towards higher EGR levels.

III. CONTROL-ORIENTED COMBUSTION MODEL

The control-oriented model used for analysis and simulations was derived from the physics-based approach by Daw *et al.* [9]. The dynamics are characterized by the in-cylinder composition, which corresponds to the residual gas from the previous combustion event and the fresh intake charge:

$$x_{k+1} = X_{\text{res}}[k]\begin{bmatrix} 1-\eta_c[k] & 0 & 0 \\ -\text{AFR}_{\text{s}}\,\eta_c[k] & 1 & 0 \\ (1+\text{AFR}_{\text{s}})\eta_c[k] & 0 & 1 \end{bmatrix} x_k + \begin{bmatrix} 1 \\ 0 \\ 0 \end{bmatrix} u_k + \begin{bmatrix} 0 & m_{\text{air,in}} & \dfrac{X_{\text{EGR}}}{1-X_{\text{EGR}}} m_{\text{air,in}} \end{bmatrix}^T \quad (1)$$

$$Q_{\text{gross}}[k] = \eta_c[k] M_{\text{fuel}}[k] Q_{\text{LHV}}. \quad (2)$$

The states $x_k = \begin{bmatrix} M_{\text{fuel}}[k] & M_{\text{air}}[k] & M_{\text{inert}}[k] \end{bmatrix}^T$ are the in-cylinder amounts of fuel, air, and inert gas. The parameters are: 1) the stoichiometric air-to-fuel ratio $\text{AFR}_{\text{s}} = 14.85$, 2) the lower heating value of the fuel $Q_{\text{LHV}} = 41$ [MJ/kg], 3) the combustion efficiency η_c, and 4) the residual gas fraction X_{res}. The fresh charge is comprised of the injected fuel command $u_k = m_{\text{fuel,in}}$, the fresh air $m_{\text{air,in}}$, and the EGR fraction X_{EGR}. Here, the cycle $k+1$ starts at IVC, which is affected by the fuel injection u_k occurring before IVC [10]. This model assumes that EGR consists only of inert gases, neglecting left-over charge in the exhaust from combustion inefficiencies. In addition, X_{EGR} and $m_{\text{air,in}}$ were assumed to be constants since they would not vary instantaneously on a cycle-to-cycle basis.

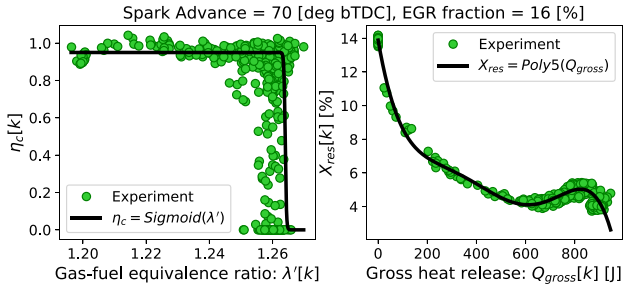

Fig. 2. Empirical correlations η_c v.s. λ' and X_{res} v.s. Q_{gross}. Solid lines correspond to the parametric models developed in [10].

Therefore, the dynamic system in Eqn. (1) has the form:

$$x_{k+1} = A_k x_k + B u_k + E \tag{3}$$

which is a linear time-variant (LTV) deterministic system. The model parameters η_c and X_{res} are affected by CCV and need to be identified from experimental data. System identification was done from in-cylinder pressure data, as demonstrated in [10]. The gross heat release was calculated from a single-zone analysis. The residual gas fraction was estimated assuming an isentropic exhaust process. It was found that the cycle-to-cycle values of $X_{\text{res}}[k]$ are very well correlated to $Q_{\text{gross}}[k]$. Similarly, $\eta_c[k]$ is correlated to the gas-fuel equivalence ratio:

$$\lambda'[k] = \frac{M_{\text{air}}[k] + M_{\text{inert}}[k]}{M_{\text{fuel}}[k]} \cdot \frac{1}{\text{AFR}_{\text{s}}}. \tag{4}$$

Under these assumptions, $\eta_c[k]$ and $X_{\text{res}}[k]$ can be written as functions of the system states, enabling offline simulations.

A. Parametric Modeling Approach

Figure 2 shows the functional dependencies used during simulations. The left plot shows $\eta_c[k]$ as a function of $\lambda'[k]$. Previous literature suggested the use of a sigmoid function to model the drop of combustion efficiency at highly diluted conditions [9]. The solid line corresponds to the sigmoid function identified in [10]. Similarly, the correlation between $X_{\text{res}}[k]$ and $Q_{\text{gross}}[k]$ can be captured by a fifth-order polynomial, as shown in the right plot of Figure 2. In a previous study, the randomness observed in the data was modeled as additive Gaussian white noise [10]. Even though this approach was able to capture the correct behavior of the observations (Q_{gross}), the simple model is not able to capture the properties of all states.

B. Non-Parametric Modeling Approach

To capture the complex behavior of η_c, consider using a conditional probability density function (PDF) identified from data. The kernel density estimator (KDE) provides a non-parametric unsupervised estimator for the conditional density $p_{X|Y}(x \mid y)$ using N observations $\{X_i, Y_i\}_{1 \le i \le N}$ as follows:

$$\widehat{p}_{X|Y}(x \mid y, h_X, h_Y) = \frac{\sum_{i=1}^{N} K\left(\frac{X_i - x}{h_X}\right) K\left(\frac{Y_i - y}{h_Y}\right)}{h_X \sum_{j=1}^{N} K\left(\frac{Y_j - y}{h_Y}\right)}. \tag{5}$$

Here, $K(z) = \frac{1}{\sqrt{2\pi}} \exp(-0.5z^2)$ is the Gaussian kernel function and $\{h_X, h_Y\}$ are the bandwidths. Such hyperparameters were chosen using the maximum-likelihood leave-one-out cross-validation. Therefore, the model parameters are treated as random variables with the following PDFs:

$$\eta_c[k] \sim \widehat{p}_{\eta|\lambda'}(\eta_c \mid \lambda'[k], h_\eta, h_{\lambda'}) \tag{6}$$

$$X_{\text{res}}[k] \sim \widehat{p}_{X|Q}(X_{\text{res}} \mid Q_{\text{gross}}[k], h_X, h_Q). \tag{7}$$

Independent values of $h_\eta, h_{\lambda'}, h_X, h_Q$ were calculated for each operating condition. The inverse cumulative distribution function (CDF) sampling was used to obtain the cycle-to-cycle values of η_c and X_{res} during simulations. Given a vector of uniform random variables $w_k = \begin{bmatrix} w_\eta[k] & w_X[k] \end{bmatrix}^T \sim \mathcal{U}(0,1)$, the simulated parameters can be obtained by evaluating the inverse CDF at the corresponding random variable as follows:

$$\eta_c[k] = \widehat{P}^{-1}_{\eta|\lambda'}(w_\eta[k]), \quad X_{\text{res}}[k] = \widehat{P}^{-1}_{X|Q}(w_X[k]). \tag{8}$$

The sequence of random variables $\{w_\eta[k]\}_{k \in \mathbb{N}}$ corresponds to in-cylinder uncertainties such as local turbulence effects, spark energy discharge, and local mixture composition. It was further assumed that such uncertainties are independent and identically distributed (iid). A similar assumption was made for the randomness in the residual gas fraction estimates. Combining the inverse CDF functions with the LTV system in Eqn. (3) results in a nonlinear time-invariant stochastic system:

$$x_{k+1} = f(x_k, u_k, w_k), \quad w_k \overset{\text{iid}}{\sim} \mathcal{U}(0,1). \tag{9}$$

C. Model Validation

Figure 3 compares the parametric model (left), nonparametric model (middle), and experimental data (right) for the most extreme condition at 16% EGR and spark advance of 70 [deg bTDC]. Return maps were used to compare the next-cycle dynamics, as well as the levels of variability observed. The top row shows the return maps corresponding to the state M_{fuel}, which displays similar behavior among the models under consideration and the data. A similar outcome resulted when comparing M_{air}. The second row depicts the return maps for M_{inert}. The in-cylinder inert mass shows a notable difference when comparing the parametric model against the experimental data. The discrepancy highlights the advantage of the nonparametric model, which is consistent across all the operating conditions presented in this letter. The return maps for Q_{gross} are shown in the bottom row since it quantifies combustion CCV. Even though all return maps look qualitatively similar, the nonparametric model shows a closer resemblance to the experiments. The Cramer-von Mises distance between the experimental and simulated CDFs of Q_{gross} (P_Q), defined as $L_2 = [\int_{\mathbb{R}} (P_Q^{\text{exp}} - P_Q^{\text{sim}})^2 dQ]^{\frac{1}{2}}$, was used to quantify how close each model mimics the data. It was found that L_2 reduces in 48% when using the nonparametric model. Hence, such a model was used to design the optimal feedback policy.

IV. Next-Cycle Optimal Control Problem

Unstable combustion events, such as partial burns and misfires, can be avoided by momentarily enriching the fresh air-fuel charge. The flame propagation, from the kernel formation to its development into a turbulent flame, depends on the laminar flame speed. For gasoline fuel, the laminar speed increases with fuel quantity and achieves its maximum at rich conditions. Higher laminar flame speed can cancel the negative

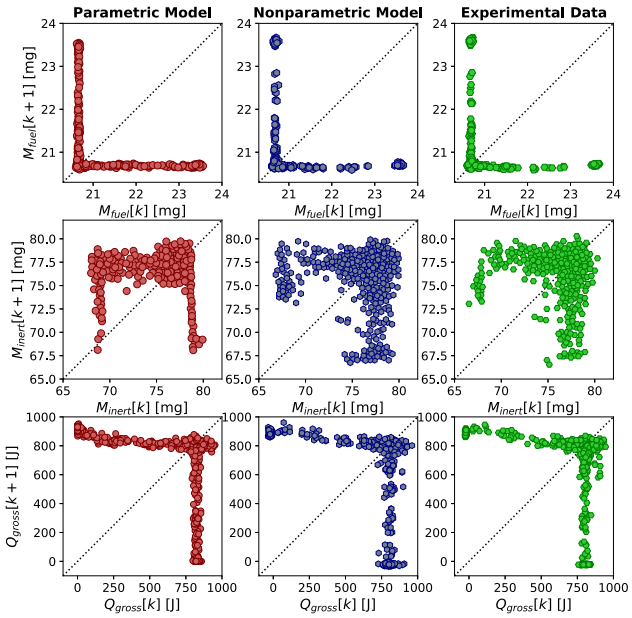

Fig. 3. Comparison between parametric model (left), nonparametric model (center), and experiment (right). Return maps: M_{fuel} (top), M_{inert} (middle), and Q_{gross} (bottom). Spark = 70 [deg bTDC] at 16% EGR.

effect EGR has on the combustion kinetics, which causes misfires. Additionally, there is a high sensitivity of the CCV with respect to fuel perturbations in the misfire region. Hence, these thermo-physical properties provide enough control authority to produce detectable effects on combustion CCV with 0.5% to 2% change in fuel injection quantity [11].

Consider now the optimal control problem of choosing the fuel injection quantity, at any cycle k, such that the following one-step-ahead expected cost function is minimized:

$$J_\rho(x_k, u_k) = \mathbb{E}\left[\left(\frac{u_k}{u_0} - 1\right)^2 + \rho\left(\frac{Q_{\text{gross}\,[k+1]}}{Q_{\text{gross},0}} - 1\right)^2\right]. \quad (10)$$

The constants u_0 and $Q_{\text{gross},0}$ are the nominal values of fuel injected and gross heat release. The first term of the cost function penalizes the deviation from u_0, which attempts to maintain as much as possible a stoichiometric charge. The second term penalizes the next-cycle deviation from $Q_{\text{gross},0}$, which is used as a measure of instantaneous CCV. The discounting factor ρ quantifies the relative importance of the future combustion CCV with respect to the present amount of fuel injected. Using the linearity of expectation and the definition of variance, Eqn. (10) can be written as:

$$J_\rho(x_k, u_k) = \left(\frac{u_k}{u_0} - 1\right)^2 + \rho\left(\frac{\mathbb{E}\big[Q_{\text{gross}}[k+1]\big]}{Q_{\text{gross},0}} - 1\right)^2 + \rho\frac{\text{Var}\big[Q_{\text{gross}}[k+1]\big]}{Q^2_{\text{gross},0}}. \quad (11)$$

According to Eqn. (2), $Q_{\text{gross}}[k+1]$ depends on the next-cycle values of the in-cylinder fuel mass and combustion efficiency. Using Eqn. (1), $M_{\text{fuel}}[k+1]$ can be calculated from the present state and control values. Therefore, finding the minimizer of Eqn. (11) requires the knowledge of the first and second moments of the random variable $\eta_c[k+1]$.

Using the KDE approach described by Eqn. (5), the first and second conditional moments can be calculated as:

$$\mathbb{E}[x \mid y, h_Y] = \sum_{i=1}^{N} K\left(\frac{Y_i - y}{h_Y}\right)X_i \Big/ \sum_{j=1}^{N} K\left(\frac{Y_j - y}{h_Y}\right) \quad (12)$$

$$\mathbb{E}[x^2 \mid y, h_X, h_Y] = \frac{\sum_{i=1}^{N} K\left(\frac{Y_i - y}{h_Y}\right)X_i^2}{\sum_{j=1}^{N} K\left(\frac{Y_j - y}{h_Y}\right)} + h_X^2. \quad (13)$$

Calculating the statistics of $Q_{\text{gross}}[k+1]$ based on Eqn. (2):

$$\begin{aligned}\mathbb{E}[Q_{\text{gross}}[k+1]] &= \mathbb{E}[\eta_c \,|\, \lambda'[k+1], h_{\lambda'}]M_{\text{fuel}}[k+1]Q_{\text{LHV}} \\ \text{Var}\,[Q_{\text{gross}}[k+1]] &= \text{Var}\,[\eta_c \,|\, \lambda'[k+1]](M_{\text{fuel}}[k+1]Q_{\text{LHV}})^2.\end{aligned} \quad (14)$$

Finally, using the definition of conditional variance:

$$\text{Var}\,[\eta_c \mid \lambda'] = \mathbb{E}[\eta_c^2 \mid \lambda'[k+1], h_\eta, h_{\lambda'}] - \mathbb{E}^2[\eta_c \mid \lambda'[k+1], h_{\lambda'}]. \quad (15)$$

According to Eqns. (4) and (1), $\lambda'[k+1]$ is a function of x_k, u_k, and the model parameters $\eta_c[k]$ and $X_{\text{res}}[k]$. By combining Eqn. (14) with the cost function $J_\rho(\cdot)$, the optimal control problem reduces to a deterministic constraint optimization with respect to the control $u_k \in \mathcal{U}$. The minimizer was found by evaluating the cost on a discretization of $\mathcal{U}$. Simulations were done in Python running on a quad-core Intel Core i7.

The control space was defined as $\mathcal{U} = [u_{\min}, u_{\max}]$. The maximum allowable amount of fuel injected is a calibration parameter ($u_{\max} = 1.06u_0$). The lower bound, however, depends on the ignition limit. A reduction of in-cylinder fuel produces a lean air-fuel mixture with reduced combustion efficiency. For simulation purposes, since the KDE depends on the collected data, consider defining the ignition limit as the maximum λ' observed during open-loop. For instance, based on the data in Figure 2, consider defining $\lambda'_{\max} = 1.27$ at 16% EGR. Such a limit depends on the level of EGR but is independent of spark advance. Therefore, at any cycle k, the control command should be chosen such that $\lambda'[k+1] \leq \lambda'_{\max}$. Using the system dynamics described by Eqn. (1) we obtained:

$$u_{\min}[k] = \frac{M_{\text{air}}[k+1] + M_{\text{inert}}[k+1]}{\lambda'_{\max} \cdot \text{AFR}_{\text{s}}} - M_{\text{fuel,res}}[k] \quad (16)$$

where $M_{\text{fuel,res}}[k] = X_{\text{res}}[k](1 - \eta_c[k])M_{\text{fuel}}[k]$. The first term of this expression calculates the in-cylinder fuel amount required to achieve $\lambda'_{\max}$. The second term corresponds to the residual unburned fuel already contained in the cylinder.

A. Control Policy

At any given cycle k, let's define the optimal control action that minimizes the expected one-step-ahead cost as follows:

$$m^*_{\text{fuel,in}}[k] = \pi_\rho(x_k) = \underset{u_k \in [u_{\min}[k], u_{\max}]}{\text{argmin}} \; J_\rho(x_k, u_k). \quad (17)$$

Calculation of the control policy $\pi_\rho(x_k)$ assumes a perfect observation of the states. In practical applications, however, it is not possible to measure the in-cylinder mass using the stock sensors. Nonetheless, a certainty equivalence approach can be adopted where Eqn. (1) generates online estimates $\widehat{x}_k$ and the

control is calculated as if they were the true states. In addition, $\pi_\rho(\cdot)$ also depends on the tunable parameter ρ. In order to relate the current problem with the theory of infinite-horizon dynamic programming, the discounting factor was restricted to $\rho \in [0, 1]$. Note that if $\rho = 0$ then $m^*_{\text{fuel,in}}[k] = u_0$, which is the open-loop control command. Therefore, if stoichiometric combustion is prioritized then the discounting factor should satisfy $\rho \to 0$. On the other hand, as $\rho \to 1$ the average fuel command will increase and the combustion CCV will be reduced. Initial simulations showed that misfires and partial burns can be avoided if $\rho = 1$, further indicating that the values of $\rho > 1$ do not need to be considered for analysis.

Previous studies showed that misfires and severe partial burns are followed by a high-energy cycle due to the high residual fuel [4], [5]. The maximum residual fuel that can be compensated by reducing $u_k \in \mathcal{U}$ can be approximated by:

$$M^{\max}_{\text{fuel,res}}[k] \approx \frac{Q_{\text{gross},0}}{Q_{\text{LHV}}} \cdot \frac{1}{\eta_0} - u_{\min}[k]. \tag{18}$$

Here, η_0 is the nominal combustion efficiency. This approximation was based on Eqn. (1) and the assumption that EGR contains no leftover fuel from previous cycles. If a low-energy event causes the residual fuel to go above $M^{\max}_{\text{fuel,res}}[k]$, then the controller requires a command lower than $u_{\min}[k]$ to achieve $Q_{\text{gross},0}$ in the following cycle. To fully use the deterministic component of CCV, consider the following augmented policy:

$$m_{\text{fuel,in}}[k] = \begin{cases} m^*_{\text{fuel,in}}[k] & \text{if } M_{\text{fuel,res}}[k] < M^{\max}_{\text{fuel,res}}[k] \\ u_{\min}[k] & \text{otherwise.} \end{cases} \tag{19}$$

This augmented policy was tested in simulations to evaluate its impact on CCV reduction and fuel injection quantity.

V. Simulation Results

Figure 4 shows the simulation results of the nonparametric model at 16% EGR and 70 [deg bTDC] spark advance for different values of ρ. The first 250 cycles were simulated in open-loop ($\rho = 0$). Every 250 cycles thereafter, during closed-loop, the discounting factor was increased according to $\rho \in \{0.01, 0.03, 1\}$. The top two plots of Figure 4 show the time series of $m_{\text{fuel,in}}[k]$ and $Q_{\text{gross}}[k]$. As expected, CCV reduces when $\rho \to 1$ as the average fuel injection quantity increases. Such fuel increase, however, is not continuous with respect to ρ and shows a switching behavior when $\rho \to 0$.

The bottom plot of Figure 4 shows the values of $\eta_c[k]$ as a function of $\lambda'[k]$. The solid and dash-dotted lines represent the conditional expectation and variance functions, respectively. The green circular markers show the experimental data used to calculate such functions according to Eqns. (12) and (13). The up triangle markers ($\triangle$) show the simulated open-loop (OL) response, which has a nominal composition of $\lambda'_0 \approx 1.26$. After a misfire occurs, the excess of in-cylinder fuel causes it to drop to $\lambda'_{\min} = 1.20$ before returning to nominal again [10]. The down triangle markers ($\triangledown$) show the closed-loop (CL) system response. In particular, the blue markers show the behavior of the system when $\rho = 0.01$. For such a value, the system shows a switching behavior between the nominal composition λ'_0 and a richer mixture of $\lambda'_{.01} \approx 1.245$. In this case, the optimal solution mimics a bang-bang controller jumping discontinuously between the OL command (u_0) and a higher value with an additional 1% fuel increase

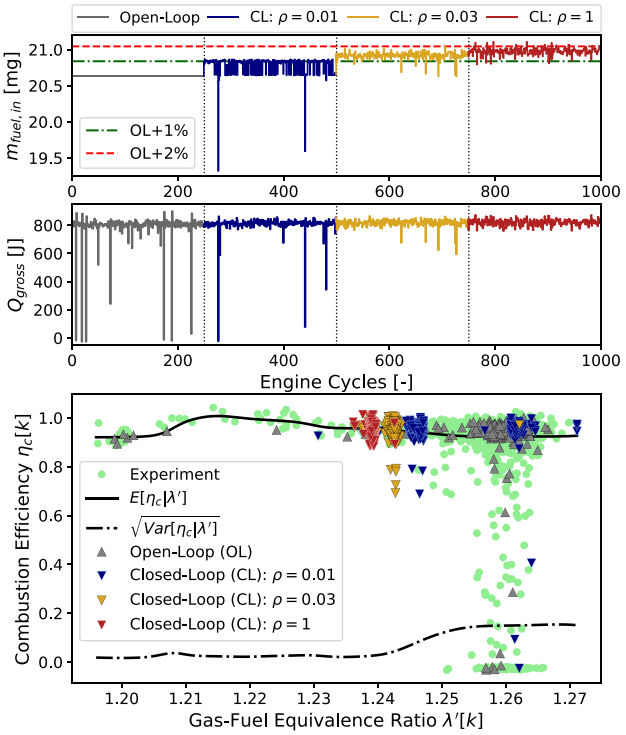

Fig. 4. Simulation results of augmented feedback control policy for several values of ρ. Top: time series of u_k. Middle: time series of Q_{gross}. Bottom: cycle-to-cycle values and statistics of η_c as function of λ'.

(OL+1%). The lower value of $\lambda'_{.01}$ provides a lower probability for misfires and partial burns compared to the nominal case, i.e., $\text{Var}[\eta_c \mid \lambda'_{.01}] < \text{Var}[\eta_c \mid \lambda'_0]$. However, the type of uncertainties encountered in the system makes it challenging to accurately predict the occurrence of low-energy events. In this simulation, for example, two of them occurred during CL operation with $\rho = 0.01$. Note that the augmented control policy immediately minimized the fuel injected to avoid the high-energy events in the next cycle. The yellow and red markers show the CL response when $\rho \in \{0.03, 1\}$, respectively. Here, the in-cylinder composition decreases continuously until $\lambda' \xrightarrow{\rho \to 1} 1.237$. At these rich conditions, the probability of low-energy events decreases rapidly as $\rho \to 1$. Therefore, misfires and partial burns can be avoided without exceeding a 2% additional fuel increase (OL+2%). All in all, Figure 4 shows the tradeoff between CCV reduction and additional fuel required for stable combustion, which is regulated by ρ. Note that, although a constant fuel command could mimic the results for $\rho \in \{0.03, 1\}$, the bang-bang behavior observed with $\rho = 0.01$ can only be achieved by a feedback control law that exploits the deterministic properties of the system.

Figure 5 shows the CoV values of IMEP and Q_{gross} during closed-loop simulations. For each condition, the discounting factor was chosen such that the additional fuel used does not exceed 1%. Comparing these results to the open-loop CCV described in Figure 1, the major reduction in CoV for both indicators occurred at advanced spark conditions. The controller is not very effective at reducing CCV at retarded conditions since CoV of Q_{gross} is already low. Nonetheless, for high levels of EGR, the CCV reduction is significant for a wide range of spark timings. At 16% EGR,

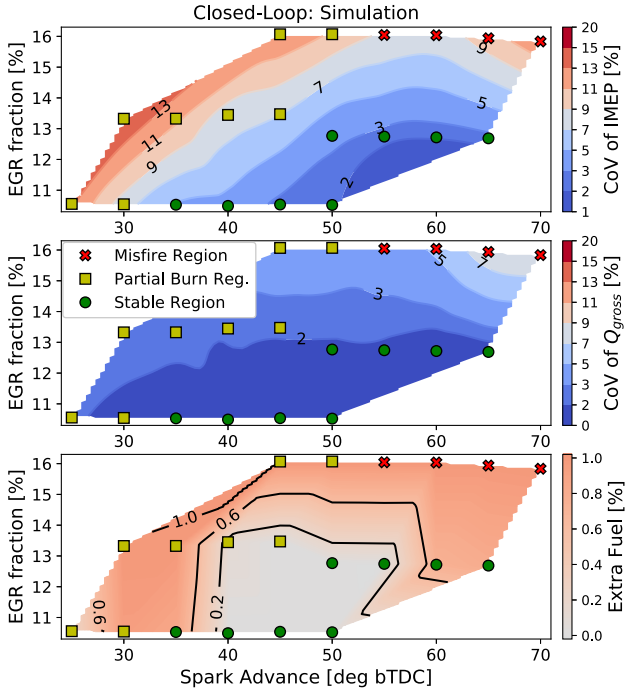

Fig. 5. Absolute value for CoV of IMEP (top) and Q_{gross} (middle) during closed-loop. Bottom: average extra fuel used for CCV reduction.

simulations showed that the controller reduced the CoV of Q_{gross} by 14% at the most retarded spark, while the reduction was 45% at the most advanced. The maximum CCV reduction was 65% for $\approx$ 63 [deg bTDC] spark advance with 13% EGR. The markers indicate the extension of the stable combustion region ($\text{CoV}_{\text{IMEP}} \leq 3\%$) by means of feedback control. The bottom plot of Figure 5 shows the average extra fuel utilized during closed-loop operation. At 16% EGR, the controller uses the allowable 1% additional fuel across conditions. At 13% EGR, however, the controller uses additional fuel only at very advanced and retarded conditions. For spark timings where CoV of Q_{gross} was low (40, 45, 50, and 55 [deg]), the discounting factor was set $\rho = 0$ in order to operate in open-loop. Similarly, at 10.5% EGR the controller was active only at retarded spark conditions where $\text{CoV}_{Q_{\text{gross}}} > 2\%$ in OL.

VI. Conclusion and Outlook

A simulation study was conducted to evaluate the potential of a next-cycle fuel injection controller to reduce CCV at high levels of EGR dilution. A physics-based model, where the carryover of residual gas affects the evolution of the system, was used for control design. The model parameters were identified from experimental data and written as functions of the states to enable offline simulations. In particular, KDEs were able to capture the stochastic properties of the states. Assuming a fully observable system, an optimal control problem was formulated that reduces CCV while minimizing the amount of extra fuel. The cost function used the discounting factor ρ to regulate the tradeoff between CCV reduction and fuel injection increase. Simulations showed that the CoV of Q_{gross} can be reduced by 65% using at most 1% additional fuel. Most of the controller benefits were found at advance spark conditions where the CoV is more sensitive to increases in EGR levels. Future research will implement this approach in a rapid prototyping engine control unit capable of cycle-to-cycle fuel control, similar to that in previous studies [8]. Experiments will also contribute to the quantification of fuel saving benefits at high EGR with the proposed feedback policy. In addition, the issue of fuel enrichment and its effect on the three-way catalyst and emissions will be experimentally analyzed. Given that a model for air-fuel ratio (AFR) was not included in this letter, the interaction between the AFR controller and the proposed next-cycle policy will be considered to maintain stoichiometric combustion while still utilizing the next-cycle fuel changes.

Acknowledgment

This research used resources at the National Transportation Research Center, a DOE-EERE User Facility at ORNL.The U.S. Government retains and the publisher, by accepting the article for publication, acknowledges that the U.S. Government retains a non-exclusive, paid-up, irrevocable, world-wide license to publish or reproduce the published form of this manuscript, or allow others to do so, for U.S. Government purposes. The DOE will provide public access to these results of federally sponsored research in accordance with the Public Access Plan.

References

[1] International Energy Agency, *Energy Technology Perspectives 2017*, OECD/IEA, Paris, France, 2017.

[2] T. Alger, J. Gingrich, C. Roberts, and B. Mangold, "Cooled exhaust-gas recirculation for fuel economy and emissions improvement in gasoline engines," *Int. J. Engine Res.*, vol. 12, no. 3, pp. 252–264, 2011.

[3] B. C. Kaul, J. B. Vance, J. A. Drallmeier, and J. Sarangapani, "A method for predicting performance improvements with effective cycle-to-cycle control of highly dilute spark ignition engine combustion," *J. Autom. Eng.*, vol. 223, no. 3, pp. 423–438, 2009.

[4] B. Kaul, R. Wagner, and J. Green, "Analysis of cyclic variability of heat release for high-EGR GDI engine operation with observations on implications for effective control," *SAE Int. J. Engines*, vol. 6, no. 1, pp. 132–141, 2013.

[5] B. Maldonado, A. Stefanopoulou, R. Scarcelli, and S. Som, "Characteristics of cycle-to-cycle combustion variability at partial-burn limited and misfire limited spark timing under highly diluted conditions," in *Proc. ASME Internal Combustion Engine Division Fall Techn. Conf.*, Oct. 2019, Art. no. v001T03A018.

[6] B. P. Maldonado, K. Zaseck, E. Kitagawa, and A. G. Stefanopoulou, "Closed-loop control of combustion initiation and combustion duration," *IEEE Trans. Control Syst. Technol.*, vol. 28, no. 3, pp. 936–950, May 2020.

[7] B. P. Maldonado and A. G. Stefanopoulou, "Cycle-to-cycle feedback for combustion control of spark advance at the misfire limit," *J. Eng. Gas Turbines Power*, vol. 140, no. 10, 2018, Art. no. 102812.

[8] B. P. Maldonado, N. Li, I. Kolmanovsky, and A. G. Stefanopoulou, "Learning reference governor for cycle-to-cycle combustion control with misfire avoidance in spark-ignition engines at high exhaust gas recirculation–diluted conditions," *Int. J. Engine Res.*, vol. 21, no. 10, pp. 1819–1834, 2020.

[9] C. S. Daw, M. B. Kennel, C. E. A. Finney, and F. T. Connolly, "Observing and modeling nonlinear dynamics in an internal combustion engine," *Phys. Rev. E, Stat. Phys. Plasmas Fluids Relat. Interdiscip. Top.*, vol. 57, pp. 2811–2819, Mar. 1998.

[10] B. P. Maldonado and B. C. Kaul, "Control-oriented modeling of cycle-to-cycle combustion variability at the misfire limit in SI engines," in *Proc. ASME Dyn. Syst. Control Conf.*, p. 11, Oct. 2020.

[11] G. S. Jatana and B. C. Kaul, "Determination of SI combustion sensitivity to fuel perturbations as a cyclic control input for highly dilute operation," *SAE Int. J. Engines*, vol. 10, no. 3, pp. 1011–1018, 2017.